

Improved anharmonic trap expansion through enhanced shortcuts to adiabaticity

C. Whitty,^{1,*} A. Kiely,^{2,3} and A. Ruschhaupt¹

¹*Department of Physics, University College Cork, Cork, Ireland*

²*School of Physics, University College Dublin, Belfield, Dublin 4, Ireland*

³*Centre for Quantum Engineering, Science, and Technology,
University College Dublin, Belfield, Dublin 4, Ireland*

Shortcuts to adiabaticity (STA) have been successfully applied both theoretically and experimentally to a wide variety of quantum control tasks. In previous work the authors have developed an analytic extension to shortcuts to adiabaticity, called enhanced shortcuts to adiabaticity (eSTA), that extends STA methods to systems where STA cannot be applied directly [Phys. Rev. Research 2, 023360 (2020)]. Here we generalize this approach and construct an alternative eSTA method that takes advantage of higher order terms. We apply this eSTA method to the expansion of both a Gaussian trap and accordion lattice potential, demonstrating the improved fidelity and robustness of eSTA.

I. INTRODUCTION

Fast high-fidelity control of quantum systems is a key requirement for the implementation of future quantum technologies [1]. Specifically, analytical control solutions are particularly desirable as they are simpler, provide greater physical insight and allow for additional stability requirements [2, 3]. Shortcuts to Adiabaticity (STA) are a broad class of analytical control techniques that mimic adiabatic evolution on much shorter timescales [4–7]. STA have been applied in many different contexts; engineering quantum heat engines [8–10], creating exotic angular momentum states in optical lattices [11], designing experimentally realizable fast driving of many-body spin systems [12], speed up STIRAP population transfer [13–16], and to inhibit unwanted transitions in two and three level systems [17].

However, STA methods can have limitations. Some STA techniques could require non-trivial physical implementation (e.g. counterdiabatic driving), while other STA techniques may only be easily applied to small or highly symmetrical systems (e.g. Lewis-Riesenfeld invariants)[5, 6]. This difficulty motivated the development of Enhanced Shortcuts to Adiabaticity (eSTA) where STA solutions can be perturbatively corrected to perform well on more complex quantum systems [18]. This method is broadly applicable, since many applications of STA techniques have already used idealized Hamiltonian descriptions e.g. single effective particles [19, 20], few-level descriptions [11, 21–23], and mean field Hamiltonians [24]. Indeed, eSTA has been applied to the transport of neutral atoms in optical conveyor belts [25, 26], and additionally has been shown to have intrinsic robustness [27].

In this work we generalize the original eSTA approach and formulate an alternative eSTA scheme. While the original eSTA scheme uses the assumption that perfect fidelity can be achieved near the starting STA scheme,

the alternative eSTA scheme does not require this assumption by using higher order terms. We show how these higher order terms can be systematically calculated using time-dependent perturbation theory.

We apply the original and alternative eSTA schemes to atomic trap expansion, using the physical settings of an optical dipole trap and an optical accordion lattice. Trap expansion of anharmonic potentials using STA has been studied [28, 29], and faster than adiabatic trap expansion has been experimentally realized using STA invariant-based engineering, in a cold atomic cloud [30], one dimensional Bose gas [31], a Fermi gas [32, 33] and loading a Bose Einstein condensate (BEC) into an optical lattice [34, 35]. The dynamic control of lattice spacing in optical accordions is another important trap expansion setting [36–38]. There have been a variety of experimental realizations of optical accordions; dynamically expanding the lattice spacing of an optical accordion loaded with ultracold atoms [39], expansion of a one dimensional BEC [40] and loading and compression of a two dimensional tunable Bose gas in an optical accordion [41].

This paper is organized as follows. In Sec. II we introduce the generalized eSTA formalism. Then we look at trap expansion in Sec. III and compare STA and eSTA control schemes, considering their sensitivity to amplitude noise in both trap models.

II. GENERALIZED ESTA FORMALISM

In the following we give a generalized derivation of eSTA, complementary to the original formalism outlined in [18], which allows the formulation of an alternate eSTA scheme.

The goal of eSTA is to control a quantum system with Hamiltonian H_s . Specifically, we want to evolve the initial state $|\Psi_0\rangle$ at time $t = 0$ to the target state $|\Psi_T\rangle$ in a given total time t_f . We assume that H_s can be approximated by an existing Hamiltonian H_0 with known STA solutions, that we refer to as the idealized STA system. In detail, we assume that there exists a parameter μ that varies continuously from μ_s to 0, such that $H_s = H_{\mu_s}$ ap-

* c.whitty@umail.ucc.ie

proaches H_0 as μ approaches 0. In later examples μ will represent the anharmonicity of the experimental trapping potential, with the idealized STA system taking the form of a time-dependent harmonic oscillator. We parameterize the control scheme of H_{μ_s} by a vector $\vec{\lambda}$, which represents the deviation from the original STA control scheme ($\vec{\lambda} = \vec{0}$). Our objective is to derive a correction to the STA scheme that improves the fidelity, which we label $\vec{\lambda}_s$.

There are two main steps behind the derivation of eSTA. The first is the assumption that μ and $\|\vec{\lambda}\|$ are small such that the fidelity landscape around ($\mu = 0, \vec{\lambda} = \vec{0}$) can be well approximated to second order in μ and $\vec{\lambda}$. Secondly, we can take advantage of the known time evolution operator of the STA system to derive an improved control scheme analytically using time-dependent perturbation theory.

A. eSTA construction

Throughout the following derivation of eSTA, we assume that at the initial and target states of H_{μ_s} can be approximated by the known eigenstates of H_0 at initial and final times. We define the fidelity

$$F(\mu, \vec{\lambda}) = \left| \langle \Psi_T | U_{\mu, \vec{\lambda}}(t_f, 0) | \Psi_0 \rangle \right|^2, \quad (1)$$

where the time evolution is explicitly parameterized by μ and $\vec{\lambda}$ through the Hamiltonian $H_{\mu}(\vec{\lambda}, t)$.

For a given H_{μ_s} we derive the eSTA control vector $\vec{\lambda}_s$ by approximating several quantities that allow us to construct a parabola in $\vec{\lambda}$ for fixed $\mu = \mu_s$. This parabola projects a path of increasing fidelity, and using the eSTA formalism we calculate the $\vec{\lambda}_s$ that corresponds to the peak of this parabola. To illustrate this construction explicitly, we let $\vec{\lambda} = \epsilon \hat{v}$ and set

$$f(\epsilon) = F(\mu_s, \epsilon \hat{v}), \quad (2)$$

with $\hat{v} = \nabla_{\vec{\lambda}} F(\mu_s, \vec{0}) / \left\| \nabla_{\vec{\lambda}} F(\mu_s, \vec{0}) \right\|$. We now approximate

$$f(\epsilon) \approx f(0) + \epsilon f'(0) + \frac{\epsilon^2}{2} f''(0), \quad (3)$$

with

$$\begin{aligned} f(0) &= F(\mu_s, \vec{0}), \\ f'(0) &= \left\| \nabla_{\vec{\lambda}} F(\mu_s, \vec{0}) \right\|, \\ f''(0) &= \hat{v}^T \text{Hess} \left[F(\mu_s, \vec{0}) \right] \hat{v}, \end{aligned} \quad (4)$$

where $\text{Hess} \left[F(\mu_s, \vec{0}) \right]$ is the Hessian matrix of second order partial derivatives of F with respect to the components of $\vec{\lambda}$, and the superscript T denotes vector transposition.

In the original eSTA approach [18], the parabola is constructed using approximations to the fidelity $F(\mu_s, \vec{0})$, the gradient $\nabla_{\vec{\lambda}} F(\mu_s, \vec{0})$, together with the assumption that the optimal control vector $\vec{\lambda}_s^{(1)}$ can achieve perfect fidelity i.e. $F(\mu_s, \vec{\lambda}_s^{(1)}) = 1$. This leads to $\epsilon_s^{(1)} = 2[1 - f(0)]/f'(0)$, with

$$\vec{\lambda}_s^{(1)} = \frac{2 \left[1 - F(\mu_s, \vec{0}) \right]}{\left\| \nabla_{\vec{\lambda}} F(\mu_s, \vec{0}) \right\|} \hat{v}. \quad (5)$$

We label this original method eSTA₁, and note that it does not use approximations to terms beyond the gradient.

Using the generalized derivation presented later in Sec. II B, we can obtain a simple approximation to the second order term $f''(0)$ in Eq. (4). Using this higher order term we derive an alternative eSTA scheme that we label eSTA₂. We construct this scheme by noting that the maximum of $f(\epsilon)$ will be at $\epsilon_s^{(2)} = -f'(0)/f''(0)$, and the eSTA₂ control vector now takes the form

$$\vec{\lambda}_s^{(2)} = - \frac{\nabla_{\vec{\lambda}} F(\mu_s, \vec{0})}{\hat{v}^T \text{Hess} \left[F(\mu_s, \vec{0}) \right] \hat{v}}. \quad (6)$$

We schematically represent the parabola construction of Eq. (3) in Fig. 1. Note that eSTA₁ (dot-dashed blue line) can overshoot the desired optimal $\vec{\lambda}_s$, due to the assumption that $F = 1$ at $\vec{\lambda}_s^{(1)}$. At the expense of calculating the Hessian term in Eq. (4) this assumption can be removed. Note that in later examples of trap expansions we will show quantitative versions of the schematic in Fig. 1.

B. Perturbative approximations for eSTA control

To calculate the eSTA control vector $\vec{\lambda}_s$ for either eSTA₁ or eSTA₂, we approximate the quantities in Eq. (4) using the known solutions to the STA system H_0 (which can be obtained for example by using invariant-based inverse engineering [4–6]) and time-dependent perturbation theory. We label the STA solutions $\{|\chi_n(t)\rangle\}$, with $|\chi_n(t)\rangle = U_{0, \vec{0}}(t, 0)|\chi_n(0)\rangle$. The time evolution operator of the STA system can be written as

$$U_{0, \vec{0}}(t, s) = \sum_{n=0}^{\infty} |\chi_n(t)\rangle \langle \chi_n(s)|. \quad (7)$$

The time evolution of a general H_{μ} can be expanded using time-dependent perturbation theory as

$$U_{\mu, \vec{\lambda}}(t, s) = U_{0, \vec{0}}(t, s) + \sum_{n=1}^{\infty} U_{\mu, \vec{\lambda}}^{(n)}(t, s), \quad (8)$$

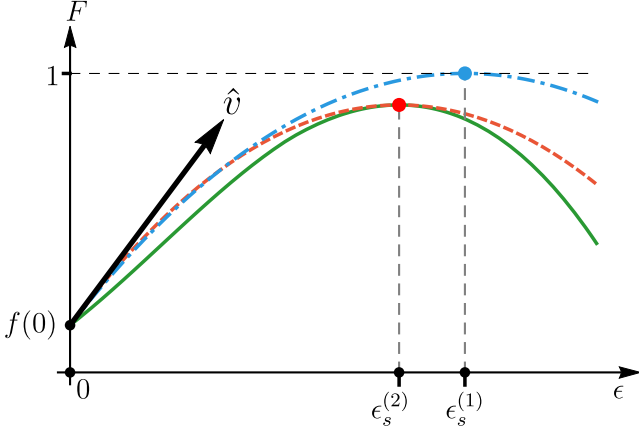


FIG. 1. (color online) Diagram of eSTA construction, $F(\mu, \epsilon \hat{v})$ vs. ϵ . The true fidelity landscape (solid green), eSTA₁ parabolic approximation (dot-dashed blue) and eSTA₂ parabola (dashed red) are shown. The normalized gradient \hat{v} is represented by the solid black arrow, and $F(\mu_s, \vec{0})$ corresponds with $f(0)$. The result of applying eSTA₂ is the improved control vector $\vec{\lambda}_s^{(2)} = \epsilon_s^{(2)} \hat{v}$, which is shown matching the peak of the true fidelity landscape well.

where

$$U_{\mu, \vec{\lambda}}^{(n)}(t_f, 0) = \left(-\frac{i}{\hbar}\right)^n \int^{(n)} U_{0, \vec{0}}(t_f, t_n) \Delta H(t_n) \dots \\ \dots U_{0, \vec{0}}(t_2, t_1) \Delta H(t_1) U_{0, \vec{0}}(t_1, 0), \quad (9)$$

and $\Delta H_\mu(\vec{\lambda}, t) = H_\mu(\vec{\lambda}, t) - H_0(\vec{0}, t)$, with the multi-integrals defined using the notation

$$\int^{(n)} \equiv \int_0^{t_f} dt_n \int_0^{t_n} dt_{n-1} \dots \int_0^{t_3} dt_2 \int_0^{t_2} dt_1. \quad (10)$$

We now set

$$\mathcal{F} = \langle \chi_0(t_f) | U_{\mu, \vec{\lambda}}(t_f, 0) | \chi_0(0) \rangle \\ = \sum_{n=0}^{\infty} \langle \chi_0(t_f) | U^{(n)}(t_f, 0) | \chi_0(0) \rangle \\ = 1 + \sum_{n=1}^{\infty} \mathcal{F}^{(n)}, \quad (11)$$

where we have used $\langle \chi_0(t_f) | U_{0, \vec{0}}(t_f, 0) | \chi_0(0) \rangle = 1$. Thus the fidelity becomes

$$F(\mu, \vec{\lambda}) = \left| \mathcal{F}(\mu, \vec{\lambda}) \right|^2 \\ = \left[1 + \sum_{n=1}^{\infty} \mathcal{F}^{(n)} \right] \left[1 + \sum_{m=1}^{\infty} \left(\mathcal{F}^{(m)} \right)^* \right] \\ = 1 + 2 \sum_{n=1}^{\infty} \text{Re} \left[\mathcal{F}^{(n)} \right] + \sum_{n=1}^{\infty} \sum_{m=1}^{\infty} \text{Re} \left[\mathcal{F}^{(n)} \left(\mathcal{F}^{(m)} \right)^* \right]. \quad (12)$$

Now we define

$$\Gamma_{n,m}(t) = \langle \chi_n(t) | \Delta H_\mu(\vec{\lambda}, t) | \chi_m(t) \rangle, \quad (13)$$

and by repeated use of Eq. (7) we have

$$\mathcal{F}^{(n)} = \left(-\frac{i}{\hbar}\right)^n \sum_{m_1=0}^{\infty} \dots \sum_{m_{n-1}=0}^{\infty} \int^{(n)} \prod_{l=0}^{n-1} \Gamma_{m_{l+1}, m_l}(t_{l+1}), \quad (14)$$

where $m_0 = m_n = 0$ and the factors in the product commute.

The advantage of this notation is that $\mathcal{F}^{(n)}$ breaks the time interval into n nested integrals, and we can collect the integrals up to second order and obtain

$$\mathcal{F}^{(1)} = -\frac{i}{\hbar} \int_0^{t_f} dt_1 \Gamma_{0,0}(t_1), \\ \mathcal{F}^{(2)} = -\frac{1}{\hbar^2} \int_0^{t_f} dt_2 \int_0^{t_2} dt_1 \sum_{m=0}^{\infty} \Gamma_{0,m}(t_2) \Gamma_{m,0}(t_1). \quad (15)$$

If we consider the fidelity up to double integrals (i.e. $n = 2$), we can write

$$F(\mu, \vec{\lambda}) \approx 1 + \frac{1}{\hbar^2} \left| \int_0^{t_f} dt \Gamma_{0,0}(t) \right|^2 \\ - \frac{2}{\hbar^2} \int_0^{t_f} dt_2 \int_0^{t_2} \sum_{m=0}^{\infty} \text{Re} [\Gamma_{m,0}^*(t_2) \Gamma_{m,0}(t_1)], \quad (16)$$

which can be simplified to

$$F(\mu, \vec{\lambda}) \approx 1 - \frac{1}{\hbar^2} \sum_{m=1}^{\infty} \left| \int_0^{t_f} dt \Gamma_{m,0}(t) \right|^2. \quad (17)$$

We derive the gradient approximation by directly taking the derivative of Eq. (17),

$$\frac{\partial F}{\partial \lambda_k} \approx -\frac{1}{\hbar^2} \sum_{m=1}^{\infty} \left[\int_0^{t_f} dt \frac{\partial}{\partial \lambda_k} \Gamma_{m,0}^*(t) \int_0^{t_f} ds \Gamma_{m,0}(s) \right. \\ \left. + \int_0^{t_f} dt \Gamma_{m,0}^*(t) \int_0^{t_f} ds \frac{\partial}{\partial \lambda_k} \Gamma_{m,0}(s) \right] \\ = -\frac{2}{\hbar^2} \sum_{m=1}^{\infty} \text{Re} \left[\int_0^{t_f} dt \frac{\partial}{\partial \lambda_k} \Gamma_{m,0}^*(t) \int_0^{t_f} ds \Gamma_{m,0}(s) \right]. \quad (18)$$

We derive an approximation to the Hessian in the same way,

$$\frac{\partial^2 F}{\partial \lambda_l \partial \lambda_k} \approx -\frac{2}{\hbar^2} \sum_{m=1}^{\infty} \text{Re} \left[\int_0^{t_f} dt \frac{\partial^2}{\partial \lambda_l \partial \lambda_k} \Gamma_{m,0}^*(t) \int_0^{t_f} ds \Gamma_{m,0}(s) \right. \\ \left. + \int_0^{t_f} dt \frac{\partial}{\partial \lambda_k} \Gamma_{m,0}^*(t) \int_0^{t_f} ds \frac{\partial}{\partial \lambda_l} \Gamma_{m,0}(s) \right]. \quad (19)$$

Note that higher order terms in these approximations are obtained using Eq. (12) and taking appropriate derivatives. We highlight that Eq. (14) allows one in principle to calculate the fidelity approximation to any order n , which will improve the approximations in Eq. (4) that are used to construct eSTA. One could even consider higher orders beyond the second order in Eq. (3), but this would require calculating more terms in the fidelity expansion of Eq. (12) and evaluating further derivatives of Eq. (12).

To calculate eSTA₁ (Eq. (5)) and eSTA₂ (Eq. (6)) explicitly, we write the fidelity and gradient approximations in terms of the notation from [18],

$$F(\mu_s, \vec{0}) \approx 1 - \frac{1}{\hbar^2} \sum_{n=1}^N |G_n|^2 =: f, \quad (20)$$

where

$$G_n = \int_0^{t_f} dt \Gamma_{n,0}(t) \Big|_{\mu=\mu_s, \vec{\lambda}=\vec{0}}, \quad (21)$$

and the gradient approximation is given by

$$\nabla_{\vec{\lambda}} F(\mu_s, \vec{0}) \approx -\frac{2}{\hbar^2} \sum_{n=1}^N \text{Re} \left(G_n^* \vec{K}_n \right) =: \vec{v}, \quad (22)$$

where the k^{th} component of \vec{K}_n is given by

$$(\vec{K}_n)_k = \int_0^{t_f} dt \frac{\partial}{\partial \lambda_k} \Gamma_{n,0}(t) \Big|_{\mu=\mu_s, \vec{\lambda}=\vec{0}}, \quad (23)$$

and we have truncated the infinite sums to the first N terms. We define

$$(W_n)_{l,k} = \int_0^{t_f} dt \frac{\partial^2}{\partial \lambda_l \partial \lambda_k} \Gamma_{n,0}^*(t) \Big|_{\mu=\mu_s, \vec{\lambda}=\vec{0}}, \quad (24)$$

and the entries of the Hessian approximation in Eq. (6) are then given by

$$\begin{aligned} \text{Hess} \left[F(\mu_s, \vec{0}) \right]_{l,k} &= \frac{\partial^2 F}{\partial \lambda_l \partial \lambda_k} \Big|_{\mu=\mu_s, \vec{\lambda}=\vec{0}} \approx \\ &- \frac{2}{\hbar^2} \sum_{n=1}^N \text{Re} \left[G_n (W_n)_{l,k} + (\vec{K}_n^*)_k (\vec{K}_n)_l \right] =: \mathbb{H}_{l,k}. \end{aligned} \quad (25)$$

Using Eq. (20), Eq. (22) and Eq. (25) we can write convenient forms for the eSTA corrections, with the improved control vector using eSTA₁ (Eq. (5))

$$\vec{\lambda}_s^{(1)} = 2(1-f) \frac{\vec{v}}{\|\vec{v}\|^2}, \quad (26)$$

and for eSTA₂ (Eq. (6)), we have

$$\vec{\lambda}_s^{(2)} = -\frac{\vec{v} \|\vec{v}\|^2}{\vec{v}^T \mathbb{H} \vec{v}}. \quad (27)$$

In the next section we apply both schemes to anharmonic trap expansion and compare the results.

III. ANHARMONIC TRAP EXPANSION

We now apply eSTA to anharmonic trap expansion and compare control protocols designed using STA, eSTA₁ and eSTA₂. Our goal is to transfer the ground state of the trap with initial trapping frequency ω_0 , to the ground state of the trap with final frequency ω_f with $\omega_f < \omega_0$. We consider two trapping potentials, a Gaussian trap and an accordion lattice. Since both potentials can be approximated by a harmonic trap near their minima, we can use a harmonic trap as the STA system from which we construct eSTA for the anharmonic systems.

A. Trap potentials

We define the accordion lattice potential as

$$V_L(x, t) = \text{sgn}[\omega_L(t)^2] A_L \sin^2[k_L(t)x], \quad (28)$$

where we write the potential with $\text{sgn}[\omega_L(t)^2]$ so that negative $\omega_L(t)^2$ corresponds to the potential changing from confining to repulsive. For the accordion lattice the wavenumber $k_L(t) = |\omega_L(t)|/\sqrt{2A_L}$ is time dependent and the amplitude constant is $A_L = \alpha[\hbar k_L(0)]^2/2m$ with α a dimensionless constant fixing the size of the recoil energy. Negative $\omega_L(t)^2$ could be implemented physically up to a global phase factor using a simple $\pi/2$ phase shift, i.e. $-A_L \sin^2[k_L(t)x] = A_L \{\sin^2[k_L(t)(x - \pi/2)] - 1\}$.

We define also the Gaussian potential as a one-dimensional approximation to an optical dipole trap [29], given by

$$V_G(x, t) = A_G(t) [1 - \exp(-k_G x^2)]. \quad (29)$$

The amplitude is time dependent, with $A_G(t) = 1/4mw^2\omega_G(t)^2$, $k_G = 2\pi/\lambda_G = 2/w^2$, m is the mass, w the beam width and λ_G is the trapping laser wavelength.

Using a series expansion of either potential, we have

$$V_{0,G/L}(x, t) = \frac{1}{2}m\omega_{G/L}(t)^2 x^2 + \mathcal{O}(x^4). \quad (30)$$

The natural choice for the STA system in the eSTA formalism for both potentials is the corresponding harmonic trap with Hamiltonian

$$H_0 = \frac{p^2}{2m} + \frac{1}{2}m\omega_{G/L}(t)^2 x^2. \quad (31)$$

Note that as the trap depth is increased for both potentials they approach the limiting case of a harmonic trap.

B. STA system and eSTA parametrization

The Hamiltonian for the STA system in Eq. (31) has a Lewis-Leach type potential with known Lewis-Riesenfeld invariant [4, 6]

$$I(t) = \frac{1}{2} \left[\frac{x^2}{b(t)^2} m\omega_0^2 + \frac{\pi(t)^2}{m} \right], \quad (32)$$

where $\pi = b(t)p - m\dot{b}x$ is the momentum conjugate to $x/b(t)$ and ω_0 is an arbitrary constant, chosen to be $\omega(0)$ for convenience. For $I(t)$ to be a dynamical invariant, $b(t)$ must satisfy the Ermakov equation

$$\ddot{b} + \omega(t)^2 b = \frac{\omega_0^2}{b^3}. \quad (33)$$

We are free to choose any $b(t)$ that satisfies the appropriate boundary conditions given by $[H(t), I(t)] = 0$ at $t = 0, t_f$:

$$\begin{aligned} b(0) &= 1, & \dot{b}(0) &= 0, & \ddot{b}(0) &= 0, \\ b(t_f) &= \gamma = \sqrt{\frac{\omega_0}{\omega_f}}, & \dot{b}(t_f) &= 0, & \ddot{b}(t_f) &= 0. \end{aligned} \quad (34)$$

Here we use a simple polynomial ansatz for $b(t)$ from [4],

$$b(t) = 6(\gamma - 1)\xi^5 - 15(\gamma - 1)\xi^4 + 10(\gamma - 1)\xi^3 + 1, \quad (35)$$

where $\xi = t/t_f$. Then $\omega(t)$ can be reverse-engineered using Eq. (33) and we obtain [4]

$$\omega(t)^2 = \frac{\omega_0^2}{b^4} - \frac{\ddot{b}}{b}. \quad (36)$$

Solutions of the Schrödinger equation $i\hbar\partial/\partial t\Psi(x, t) = H_0\Psi(x, t)$ can be written as,

$$\Psi(x, t) = \sum_{n=0}^{\infty} c_n e^{i\theta_n(t)} \psi_n(x, t), \quad (37)$$

where $\psi_n(x, t)$ are orthonormal eigenstates of the invariant I satisfying $I(t)\psi_n(x, t) = \lambda_n\psi_n(x, t)$ and c_n are constants, with the Lewis-Riesenfeld phase given by

$$\theta_n(t) = \frac{1}{\hbar} \int_0^t \langle \phi(t', n) | i\hbar \frac{\partial}{\partial t'} - H_0(t') | \phi(t', n) \rangle dt'. \quad (38)$$

For harmonic trap expansion, a single mode in Eq. (37) is given by

$$\chi_n(x, t) = e^{i\theta_n(t)} e^{i\beta_n(x, t)} \frac{\phi_n(x/b)}{b^{1/2}} \quad (39)$$

where

$$\begin{aligned} \theta_n(t) &= -(n + 1/2) \int_0^t dt' \frac{\omega_0}{b(t')^2}, \\ \beta_n(x, t) &= \frac{m}{2\hbar} \frac{\dot{b}}{b(t)} x^2, \end{aligned} \quad (40)$$

with $\lambda_n = (n + 1/2)\hbar\omega_0$, and $\phi_n(x)$ are harmonic energy eigenstates.

In Fig. 2, $\omega^2(t)/\omega_0^2$ is shown for several different final times t_f . Note that even though the trap frequency can become negative, there are techniques that allow negative potentials to be implemented experimentally [4]. From

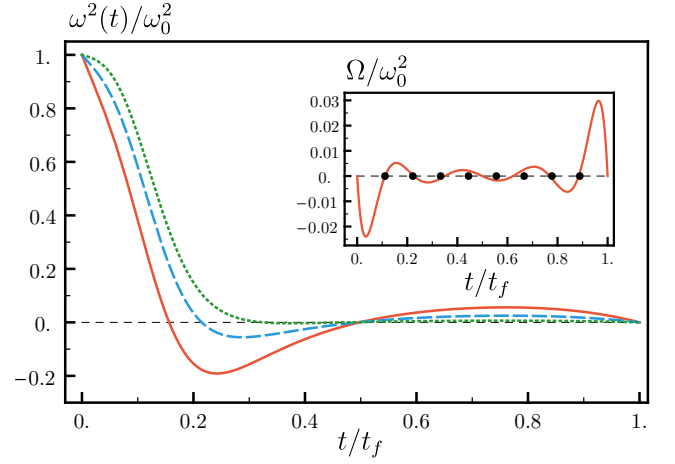


FIG. 2. Examples of $\omega^2(t)/\omega_0^2$ using $\gamma = 10$, with $\omega_0 t_f = 10$ (solid-red), 15 (dashed-blue), and 30 (dotted-green). Inset: Example of Ω with $\tau_L = 26$ for fast lattice expansion using eSTA₂, with black dots indicating $M = 8$ parameterization of Eq. (42).

Eq. (36) we obtain the STA solution $\omega(t)^2$ that we use as a starting point to construct the eSTA solution

$$\tilde{\omega}(t)^2 = \omega(t)^2 + \Omega(\vec{\lambda}, t), \quad (41)$$

where for convenience we choose the eSTA correction Ω to be a polynomial that satisfies $\Omega(\vec{\lambda}, 0) = 0$ and $\Omega(\vec{\lambda}, t_f) = 0$. We parameterize Ω by the vector $\vec{\lambda} = (\lambda_1, \dots, \lambda_M)$, where

$$\Omega\left(\vec{\lambda}, \frac{j t_f}{M+1}\right) = \lambda_j, \quad j = 1, \dots, M, \quad (42)$$

and M is the number of components in $\vec{\lambda}$.

Now we use eSTA to calculate the value of $\vec{\lambda}$ that improves the fidelity. In detail, we calculate $\vec{\lambda}_s^{(1)}$ using Eq. (26) (eSTA₁) and $\vec{\lambda}_s^{(2)}$ using Eq. (27) (eSTA₂). These formulae require calculating Eq. (21), Eq. (23) and Eq. (25).

First we calculate G_n from Eq. (21) using

$$\begin{aligned} G_n &= \int_0^{t_f} dt \Gamma_{n,0}(t) \Big|_{\mu=\mu_s, \vec{\lambda}=\vec{0}} \\ &= \int_0^{t_f} dt \langle \chi_n(t) | \Delta H_{\mu_s}(\vec{0}, t) | \chi_0(t) \rangle, \end{aligned} \quad (43)$$

where $|\chi_n(t)\rangle$ is given by Eq. (39) and $\Delta H_{\mu_s} = H_{\mu_s} - H_0 = V_{G/L} - V_{0,G/L}$, with H_0 from Eq. (31), $V_{G/L}$ from Eq. (29) and Eq. (28), and $V_{0,G/L}$ from Eq. (30). To calculate the k^{th} component of \vec{K}_n from Eq. (23), we

have

$$\begin{aligned}
(\vec{K}_n)_k &= \int_0^{t_f} dt \frac{\partial}{\partial \lambda_k} \Gamma_{n,0}(t) \Big|_{\mu_s, \vec{\lambda}=\vec{0}} \\
&= \int_0^{t_f} dt \langle \chi_n(t) | \frac{\partial}{\partial \lambda_k} \Delta H_{\mu_s}(\vec{\lambda}, t) \Big|_{\vec{\lambda}=\vec{0}} | \chi_0(t) \rangle \\
&= \int_0^{t_f} dt \langle \chi_n(t) | \frac{\partial}{\partial \lambda_k} V_{G/L} \Big|_{\vec{\lambda}=\vec{0}} | \chi_0(t) \rangle. \quad (44)
\end{aligned}$$

In a similar manner we evaluate Eq. (25) that is required only for calculating $\vec{\lambda}_s^{(2)}$. An example of the resulting eSTA correction $\Omega(\vec{\lambda}, t)$ for fast expansion of the accordion lattice using $\vec{\lambda}_s^{(2)}$ with $M = 8$ components is shown in the inset of Fig 2.

C. Fidelity Results: Accordion Lattice Expansion

We first apply eSTA to the expansion of an accordion lattice with a single trapped ^{133}Cs atom in the ground state. We set the lattice parameters using values from an experimentally implemented optical lattice [42], where the initial wavenumber is $k_L(0) = 2\pi/\lambda_L$ and using Eq. (30) we have that $\omega_{0,L} = \omega_L(0) = 4\sqrt{\alpha}\pi^2\hbar/m\lambda_L^2$. We use numerical values $\lambda_L = 866\text{nm}$ and recoil energy parameter $\alpha = 150$ [42]. We set the dimensionless final time $\tau_L = \omega_{0,L}t_f$ and have that $A_L/\hbar\omega_{0,L} \approx 6.12$.

We calculate the fidelity for different expansion times τ_L . In Fig. 3 (a) the results for STA, eSTA₁ and eSTA₂ are shown. For both $\vec{\lambda}_s^{(1)}$ and $\vec{\lambda}_s^{(2)}$ we use $M = 1$ and $M = 8$ components ($M = 1$ and $M = 8$ in Eq. (42) resp.). Calculating eSTA requires truncating the sums in Eq. (21), Eq. (23) and Eq. (24). For the results in this paper we use the first four non-zero terms.

We find that eSTA₂ gives improvement over eSTA₁ and STA as expected. The 8 component schemes show improvement over 1 component schemes, for both eSTA₁ and eSTA₂. This demonstrates that $\vec{\lambda}_s$ with only a few components can produce significant fidelity improvement, particularly when using eSTA₂.

In the derivation of eSTA₁ it was assumed that the system could achieve maximum fidelity, i.e. $F(\mu_s, \vec{\lambda}_s^{(1)}) = 1$. The inset of Fig. 3 (a) demonstrates that this can lead to overshooting, which we previously illustrated schematically in Fig. 1; here we consider eSTA₁ and eSTA₂ with only 1 component, for $\tau_L = 25$. The true fidelity landscape (solid-green), eSTA₁ (dotted-blue) and eSTA₂ (dashed-red) fidelity approximations are shown, with the eSTA₁ scheme minimally overshooting the optimal ϵ_s . We find that $\epsilon_s^{(1)}$ from eSTA₁ is approximately $1.5 \times \epsilon_s^{(2)}$. Note that both versions of eSTA would agree if the fidelity for both $\vec{\lambda}_s^{(1)}$ and $\vec{\lambda}_s^{(2)}$ was exactly 1. We note that calculating eSTA₁ may be simpler than calculating eSTA₂ in certain settings, and that the utility of either eSTA approach will depend on the given system dynamics.

D. Fidelity Results: Gaussian Trap Expansion

We consider Gaussian trap expansion and use similar values to the Gaussian approximation of a single trapped ^{87}Rb atom in an optical dipole trap in [28, 29], with inverse unit of time $\omega_{0,G} = 2\pi \times 2500\text{Hz}$, $A_G/\hbar\omega_{0,G} \approx 2418$, laser wavelength $\lambda_{\text{laser}} = 1060\text{nm}$, a beam waist of $20\lambda_{\text{laser}}$ and set the expansion time $\tau_G = \omega_{0,G}t_f$.

We simulate Gaussian trap expansion for different expansion times τ_G and the results are shown in Fig. 3 (b), using the STA scheme (solid-green line), eSTA₁ (dotted and solid blue lines) and eSTA₂ (dashed and solid red lines).

As with the optical accordion, we consider eSTA₁ and eSTA₂ with two parameterizations of $\vec{\lambda}_s^{(1)}$ and $\vec{\lambda}_s^{(2)}$, a 1 component scheme (dotted-blue, dashed-red) and an 8 component scheme (solid blue, solid red). We find that eSTA₁ and eSTA₂ are an improvement over STA, and that the 1 and 8 component schemes produce very similar results for both eSTA₁ and eSTA₂. This is an indication that the polynomial form of $\Omega(\vec{\lambda}, t)$ allows a large class of improved schemes. The inset of Fig. 3 (b) demonstrates again that the original eSTA scheme can minimally overshoot the optimal ϵ_s (compare again to Fig. 1), with the parabola calculated using eSTA₂ matching the true fidelity well.

E. ESTA Sensitivity

In this section we consider errors in the trapping potentials and calculate the sensitivity to these errors using the STA, eSTA₁ and eSTA₂ schemes introduced earlier. For the lattice potential we consider an error in the amplitude

$$V_{\text{err}}^L(x, t) = \text{sgn}[\omega_L(t)^2] A_L(1 + \delta) \sin^2[k_L(t)x], \quad (45)$$

and for the Gaussian potential we also consider an amplitude error, given by

$$V_{\text{err}}^G(x, t) = A_G(1 + \delta) \{1 - \exp^2[-k_G(t)x^2]\}. \quad (46)$$

We define the error sensitivity by

$$S := \left| \frac{\partial F}{\partial \delta} \right|_{\delta=0}, \quad (47)$$

and calculate this quantity numerically using a multi-point discrete approximation to the derivative. Note that a lower sensitivity S means a given scheme is more robust against error.

Heuristically we expect that eSTA will simultaneously improve fidelity and robustness: for $\mu = 0$ both eSTA and STA give fidelity 1, and as μ increases the eSTA fidelity is always higher than the STA fidelity, i.e. the slope of the eSTA fidelity is expected to be smaller than the slope of the STA scheme. Assuming that this slope is

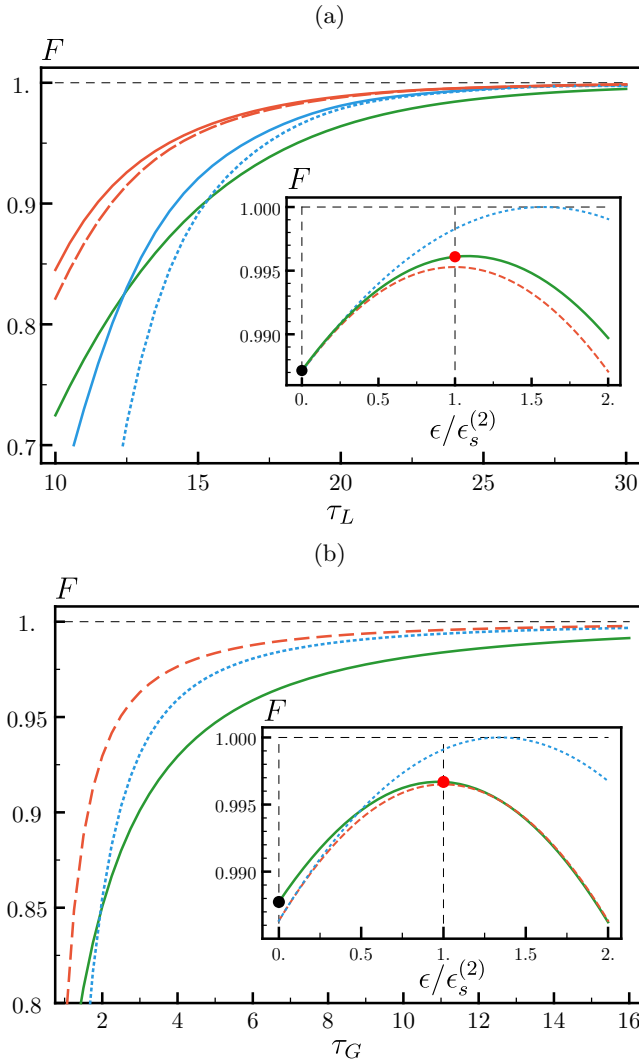


FIG. 3. Fidelity vs. expansion time $\tau_{L/G}$. (a) Lattice expansion; STA (solid green), eSTA₁ with $M=8$ components (solid blue) and $M=1$ (dotted blue), eSTA₂ $M=8$ (solid red) and $M=1$ (dashed red). Lattice parameters as in Sec. III C for this plot and the inset.

Inset: Fidelity vs $\epsilon/\epsilon_s^{(2)}$ for lattice expansion with $\tau_L = 25$; true fidelity landscape (solid green), eSTA₁ (dotted blue) and eSTA₂ (dashed red) parabola approximations.

(b) Gaussian trap expansion; same labeling as (a), with $M=1$ and $M=8$ results indistinguishable (solid lines omitted). Physical values given in Sec. III D. Inset: Same labeling as (a) with $\tau_G = 13$.

approximately proportional to the error sensitivity S , we also expect lower error sensitivity for eSTA than STA.

In the following we look at the numerical error sensitivity. In Fig 4 (a) the sensitivity of lattice expansion is shown, with STA (dot-dashed green), eSTA₁ ($M=1$ dotted-blue, $M=8$ solid blue) and eSTA₂ ($M=1$ dashed-red, $M=8$ solid red). Each line is marked at the point where $F \geq 0.95$, with eSTA₁ and eSTA₂ still achieving this fidelity for lower τ_L than STA. In this

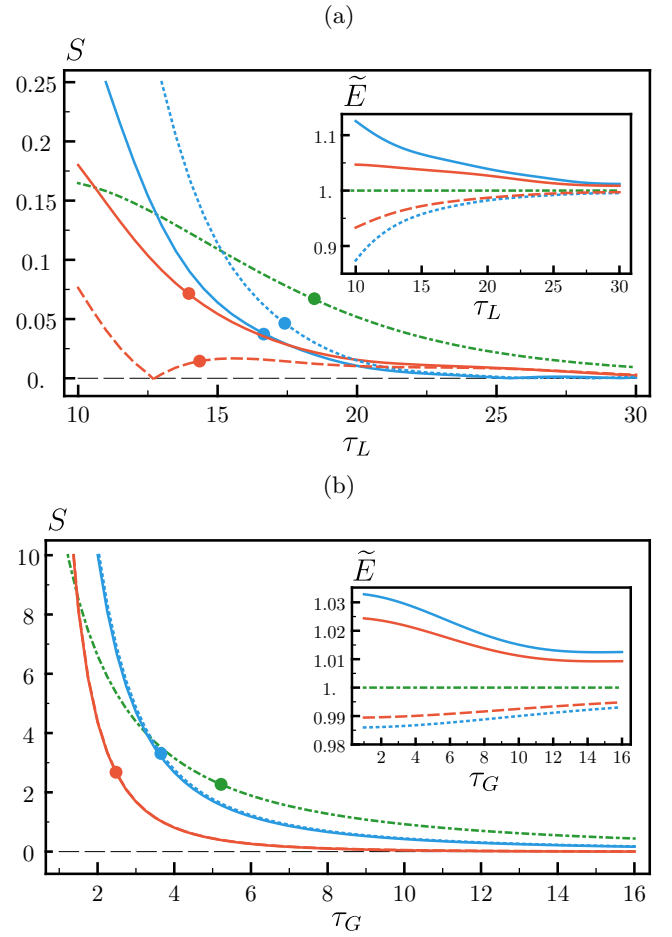


FIG. 4. Trap expansion sensitivity $S = |\partial F / \partial \delta|$ vs. $\tau_{L/G}$. Same parameters and labeling as Fig 3. (a) Lattice expansion, with first τ_L for which $F > 0.95$ marked on each line. Inset: Time averaged energy (Eq. (48)) of the eSTA schemes scaled by the STA scheme (dot-dashed green), \tilde{E} vs. τ_L . (b) Gaussian trap expansion sensitivity S vs. τ_G , again with first τ_G for which $F > 0.95$ shown.

high fidelity regime, both eSTA schemes are generally less sensitive (smaller S) to error than the STA scheme for $\tau_L \gtrsim 15$, in agreement with the heuristic argument from above. The eSTA₂ scheme generally gives the highest fidelities and lowest sensitivities, as shown in Fig. 3 (a) and Fig. 4 (a). Interestingly, the single component ($M=1$) eSTA₂ scheme (dashed-red line) has lower sensitivity than the 8 component ($M=8$) eSTA₂ scheme (solid-red line).

For Gaussian trap expansion, see Fig. 4 (b), there is negligible difference in sensitivity between choosing a single or 8 component scheme, for either eSTA₁ or eSTA₂. Again, the points for which $F \geq 0.95$ is first achieved are marked on each line. For these high fidelities eSTA₁ and eSTA₂ outperform STA, in agreement with the heuristic argument outlined earlier. In this case eSTA₂ has generally the highest fidelity, as shown in Fig. 3 (b), as well as

the lowest sensitivity in Fig. 4 (b). A convenient eSTA scheme can be chosen depending on the required fidelity or sensitivity.

We also consider the time averaged energy

$$E(\vec{\lambda}) = \frac{1}{t_f} \int_0^{t_f} dt \langle H_{\mu_s}(\vec{\lambda}, t) \rangle, \quad (48)$$

and define $\tilde{E} = E(\vec{\lambda})/E(\vec{0})$ such that the different eSTA protocols are in direct comparison with the STA scheme. The insets in Fig. 3 (a) and (b) show \tilde{E} for eSTA₁ and eSTA₂. The values of \tilde{E} of the eSTA schemes are close to 1 (i.e. close to the STA scheme), demonstrating that little additional time averaged energy is required for improvement. In both lattice and Gaussian expansion, the 1 component STA schemes have a lower time averaged energy than STA ($\tilde{E} < 1$), while using more components ($M = 8$) has a higher value ($\tilde{E} > 1$).

IV. CONCLUSION

The main result in this paper is a generalization of the original eSTA derivation in [18], and the construction of an alternative eSTA scheme. This alternative eSTA scheme allows the removal of an assumption of the original eSTA method, at the expense of calculating an additional Hessian term. Both eSTA schemes are applied to anharmonic trap expansion, resulting in higher fidelity and improved robustness.

Generally, there are several important advantages that

the eSTA formalism has to offer; the derivation is analytic, applicable to a wide variety of quantum control problems and the control schemes are expected to have enhanced robustness against noise. In addition, eSTA can offer insight into a given control problem, for example by first considering low dimension parameterizations of the control scheme. There is also significant freedom in choosing how to parameterize the control scheme for either approach; for example, we can choose to preserve the symmetry of the original STA scheme, or use a form of the eSTA improvement that lends itself to certain conditions e.g. a Fourier sum with fixed bandwidth. Analytic eSTA control schemes that are outside the class of STA solutions can be derived, and they could give improved starting points for numerical optimization. As an outlook, higher order eSTA schemes can be constructed using the formalism presented in this paper which would be useful if some lower order terms vanish.

ACKNOWLEDGMENTS

We are grateful to D. Rea and J. Li for their fruitful discussion and careful reading of the manuscript. C.W. acknowledges support from the Irish Research Council (GOIPG/2017/1846). A.K. acknowledges support from the Science Foundation Ireland Starting Investigator Research Grant “SpeedDemon” No. 18/SIRG/5508. A.R. acknowledges support from the Science Foundation Ireland Frontiers for the Future Research Grant “Shortcut-Enhanced Quantum Thermodynamics” No. 19/FFP/6951.

-
- [1] S. J. Glaser, U. Boscain, T. Calarco, C. P. Koch, W. Köckenberger, R. Kosloff, I. Kuprov, B. Luy, S. Schirmer, T. Schulte-Herbrüggen, D. Sugny, and F. K. Wilhelm, *Eur. Phys. J. D* **69**, 279 (2015).
 - [2] A. Ruschhaupt, X. Chen, D. Alonso, and J. G. Muga, *New J. Phys.* **14**, 093040 (2012).
 - [3] A. Kiely, J. P. L. McGuinness, J. G. Muga, and A. Ruschhaupt, *J. Phys. B: At. Mol. Opt. Phys.* **48**, 075503 (2015).
 - [4] X. Chen, A. Ruschhaupt, S. Schmidt, A. del Campo, D. Guéry-Odelin, and J. G. Muga, *Phys. Rev. Lett.* **104**, 063002 (2010).
 - [5] E. Torrontegui, S. Ibáñez, S. Martínez-Garaot, M. Modugno, A. del Campo, D. Guéry-Odelin, A. Ruschhaupt, X. Chen, and J. G. Muga, *Adv. At., Mol., Opt.* **62**, 117 (2013).
 - [6] D. Guéry-Odelin, A. Ruschhaupt, A. Kiely, E. Torrontegui, S. Martínez-Garaot, and J. G. Muga, *Rev. Mod. Phys.* **91**, 045001 (2019).
 - [7] A. del Campo and K. Kim, *New J. Phys.* **21**, 050201 (2019).
 - [8] A. del Campo, J. Goold, and M. Paternostro, *Sci Rep* **4**, 6208 (2014).
 - [9] A. del Campo, A. Chenu, S. Deng, and H. Wu, in *Thermodynamics in the Quantum Regime: Fundamental Aspects and New Directions*, edited by F. Binder, L. A. Correa, C. Gogolin, J. Anders, and G. Adesso (Springer International Publishing, Cham, 2018) pp. 127–148.
 - [10] J. Li, T. Fogarty, S. Campbell, X. Chen, and T. Busch, *New J. Phys.* **20**, 015005 (2018).
 - [11] A. Kiely, A. Benseny, T. Busch, and A. Ruschhaupt, *J. Phys. B: At. Mol. Opt. Phys.* **49**, 215003 (2016).
 - [12] H. Saberi, T. Opatrny, K. Mølmer, and A. del Campo, *Phys. Rev. A* **90**, 060301 (2014).
 - [13] M. Demirplak and S. A. Rice, *J. Phys. Chem. A* **107**, 9937 (2003).
 - [14] K. Bergmann, N. V. Vitanov, and B. W. Shore, *J. Chem. Phys.* **142**, 170901 (2015).
 - [15] S. Masuda and S. A. Rice, *J. Phys. Chem. A* **119**, 3479 (2015).
 - [16] N. V. Vitanov, A. A. Rangelov, B. W. Shore, and K. Bergmann, *Rev. Mod. Phys.* **89**, 015006 (2017).
 - [17] A. Kiely and A. Ruschhaupt, *J. Phys. B: At. Mol. Opt. Phys.* **47**, 115501 (2014).
 - [18] C. Whitty, A. Kiely, and A. Ruschhaupt, *Phys. Rev. Research* **2**, 023360 (2020).
 - [19] B. Juliá-Díaz, E. Torrontegui, J. Martorell, J. G. Muga, and A. Polls, *Phys. Rev. A* **86**, 063623 (2012).

- [20] A. Kiely and S. Campbell, *New J. Phys.* **23**, 033033 (2021).
- [21] S. Martínez-Garaot, E. Torrontegui, X. Chen, M. Modugno, D. Guéry-Odelin, S.-Y. Tseng, and J. G. Muga, *Phys. Rev. Lett.* **111**, 213001 (2013).
- [22] A. Benseny, A. Kiely, Y. Zhang, T. Busch, and A. Ruschhaupt, *EPJ Quantum Technol.* **4**, 1 (2017).
- [23] Y.-C. Li, X. Chen, J. G. Muga, and E. Y. Sherman, *New J. Phys.* **20**, 113029 (2018).
- [24] K. Takahashi, *Phys. Rev. A* **95**, 012309 (2017).
- [25] S. H. Hauck, G. Alber, and V. M. Stojanović, *Phys. Rev. A* **104**, 053110 (2021).
- [26] S. H. Hauck and V. M. Stojanović, **18**, 014016.
- [27] C. Whitty, A. Kiely, and A. Ruschhaupt, *Phys. Rev. A* **105**, 013311 (2022).
- [28] E. Torrontegui, X. Chen, M. Modugno, A. Ruschhaupt, D. Guéry-Odelin, and J. G. Muga, *Phys. Rev. A* **85**, 033605 (2012).
- [29] X.-J. Lu, X. Chen, J. Alonso, and J. G. Muga, *Phys. Rev. A* **89**, 023627 (2014).
- [30] J.-F. Schaff, X.-L. Song, P. Vignolo, and G. Labeyrie, *Phys. Rev. A* **82**, 033430 (2010).
- [31] W. Rohringer, D. Fischer, F. Steiner, I. E. Mazets, J. Schmiedmayer, and M. Trupke, *Sci Rep* **5**, 9820 (2015).
- [32] S. Deng, P. Diao, Q. Yu, A. del Campo, and H. Wu, *Phys. Rev. A* **97**, 013628 (2018).
- [33] S. Deng, A. Chenu, P. Diao, F. Li, S. Yu, I. Coulamy, A. del Campo, and H. Wu, *Science Advances* **4**, eaar5909 (2018).
- [34] S. Masuda, K. Nakamura, and A. del Campo, *Phys. Rev. Lett.* **113**, 063003 (2014).
- [35] X. Zhou, S. Jin, and J. Schmiedmayer, *New J. Phys.* **20**, 055005 (2018).
- [36] R. A. Williams, J. D. Pillet, S. Al-Assam, B. Fletcher, M. Shotton, and C. J. Foot, *Opt. Express*, OE **16**, 16977 (2008).
- [37] T. C. Li, H. Kelkar, D. Medellin, and M. G. Raizen, *Opt. Express*, OE **16**, 5465 (2008).
- [38] J. Tao, Y. Wang, Y. He, and S. Wu, *Opt. Express*, OE **26**, 14346 (2018).
- [39] S. Al-Assam, R. A. Williams, and C. J. Foot, *Phys. Rev. A* **82**, 021604 (2010).
- [40] L. Fallani, C. Fort, J. E. Lye, and M. Inguscio, *Opt. Express*, OE **13**, 4303 (2005).
- [41] J. L. Ville, T. Bienaimé, R. Saint-Jalm, L. Corman, M. Aidelsburger, L. Chomaz, K. Kleinlein, D. Perconte, S. Nascimbène, J. Dalibard, and J. Beugnon, *Phys. Rev. A* **95**, 013632 (2017).
- [42] M. R. Lam, N. Peter, T. Groh, W. Alt, C. Robens, D. Meschede, A. Negretti, S. Montangero, T. Calarco, and A. Alberti, *Phys. Rev. X* **11**, 011035 (2021).